Lithium excitation by slow H^+ and He^{2+} ions

J. W. Turkstra,[1] D. Meyer,[1] R. Hoekstra,[1] R. Morgenstern,[1] and J. Schweinzer[2]
[1]*KVI Atomic Physics, Zernikelaan 25, 9747 AA Groningen, The Netherlands*
[2]*Max-Planck-Institut für Plasmaphysik, Boltzmannstraße 2, D-85748 Garching, Germany*
(Received 28 June 1999)

Experimental and theoretical cross sections for the excitation of ground-state lithium by H^+ and He^{2+} impact are presented for the 2–30 keV/amu energy regime. Li($2s$) excitation up to the Li($n=4$) level was simulated by means of the atomic-orbital close-coupling method. Experimentally, absolute emission cross sections were determined by observing the LiI(nd-$2p$,$n=3$–6) and LiI(ns-$2p$,$n=4$–6) line radiation after ion impact. Furthermore, a few measurements have been performed on high-n excitation [Li($2s\rightarrow nd$,$n=7$–9)] by He^{2+} impact. [S1050-2947(99)06912-7]

PACS number(s): 34.50.Fa, 34.10.+x

I. INTRODUCTION

In the field of ion-atom collisions, the one-electron and quasi-one-electron targets (H, Li, Na, etc.) have always received a lot of attention. Most attention was usually directed to single electron capture, because it is a process that can be described by various models at different levels of sophistication: over-the-barrier [1], multichannel Landau-Zener [2], classical-trajectory Monte Carlo (CTMC) [3,4] and atomic-orbital close-coupling (AOCC) [5]. However, for the description of target excitation and ionization, most models are not so well suited, mainly because electron capture dominates over the other processes, especially in the low-energy region. Also there was a lack of experiments to test and improve the various models. For lithium target excitation the experimental work consisted of experiments by Kadota *et al.* [6] and Aumayr *et al.* [7,8] and theoretical studies were done by Ermolaev *et al.* [9] and Schweinzer *et al.* [10]. Other closely related studies have been performed by Fritsch *et al.* [11], Schultz *et al.* [12] (hydrogen excitation), and Horvath *et al.* [13] (sodium excitation).

In this work we present a study on

$$(H^+,He^{2+})+Li(2s)\rightarrow(H^+,He^{2+})+Li^*(n,l)\rightarrow(H^+,He^{2+})+Li(2s)+h\nu \quad (1)$$

by means of photon emission spectroscopy (experiment) and AOCC (theory). This work has an intended overlap with another body of work (on lithium excitation by ion impact) performed recently by Brandenburg *et al.* [14]. Together with this work, a consistent, reasonably complete picture on lithium excitation can be constructed with some unexpected features, most of them supported by the AOCC theory.

Another important motivation for this work was to construct a high-quality database of lithium excitation by ion impact to be used for the lithium beam diagnostics of magnetically confined fusion plasmas [16]. The previous lithium excitation database mainly consisted of scaled electron impact cross sections [17], which are not likely to describe ion-atom collisions very well in the low-energy region (1–20 keV/amu) because the coupling between excitation channels and electron capture channels is not incorporated. Therefore a new database [18] including all collision processes relevant for the plasma diagnostic purpose has been compiled recently. The ion-impact part of this new database is based on the AOCC calculations presented here.

II. THEORY

We applied the well-known semiclassical impact-parameter formulation of the close-coupling (CC) method for collisions with one ''active'' electron, assuming straight line trajectories for the projectiles. The general approach has already been described by Horvath *et al.* [13] (and references therein), which shall not be repeated here. Only details for the particularly chosen two-center expansions will be given which are of importance for the discussions in the following sections. All chosen basis sets used in the present CC calculation are listed in Table I. This table has to be regarded just as a survey, and detailed information about the used basis set is available from the authors on request. Besides atomic orbitals (AOs) on projectile and target, pseudostates on both centers appear in the expansion. While AOs on the projectile (H^++, He^{2+}) are simply given by hydrogenic states, AOs for Li are derived by diagonalizing the atomic Hamiltonian in a truncated basis set of Slater-type orbitals (STOs, defined by charge z and n,l quantum numbers). The Hamiltonian on the Li center includes an analytic model potential [20] for the interaction between the Li^+ core and the ''active'' electron. The diagonalization process leads to linear combinations of the original STOs which represent AOs in cases where the corresponding eigenvalues are close to experimental energy levels (deviations $<0.3\%$). All other eigenstates of the diagonalization process are called pseudostates (PSs) and their eigenvalues cover a range of energies above the highest AO state to positive values. Such states are considered—though of discrete nature—to represent the continuum in the calculation. One can further distinguish between such STOs optimized in order to reproduce most accurately the atomic level diagram (PS-ST, where ST stands for structure) and STOs with z values (not given in Table I) between the charge of the separated atoms and the united atom (PS-UA). The latter are more appropriate for small impact parameters to describe the motion of the active electron. The eigenvalues of these PS-UA lie above the AOs and represent higher excited

TABLE I. Basis sets used in the AOCC simulations.

	Center on projectile Z^{q+}		Center on target Li^+		
Calculation	AO	PS-UA	AO	PS-ST	PS-UA
H^+					
ao65_64	20; $n=1-4$	45 STO $l\leqslant 4$	20; $n=1-4$	17 STO $l\leqslant 1$	27 STO $2\leqslant l\leqslant 4$
He^{2+}					
ao87_79	56; $n=1-6$	31 STO $1\leqslant l\leqslant 4$	35; $n=1-5$	17 STO $l\leqslant 1$	27 STO $2\leqslant l\leqslant 4$
ao81_80	50; $n=1-5, 6l\leqslant 4$	31 STO $1\leqslant l\leqslant 4$	35; $n=1-5$	14 STO $l\leqslant 1$	31 STO $1\leqslant l\leqslant 4$

bound states as well as ionization channels. This type of state (PS-UA) is also included at the projectile center representing capture to the continuum. All presented AO calculations (e.g., Table I) involve a considerable number of projectile centered states representing single electron capture (SEC). The importance of such channels for the results of excitation cross sections has already been discussed for the Li($2s$-$2p$) excitation in He^{2+}-Li($2s$) collisions [10]. In this pure AOCC study (no pseudostates were included) the number of included SEC channels influenced the resulting excitation cross section significantly in the lower impact energy range. Furthermore it turned out that, in order to obtain reasonable results, it is recommended to include SEC from the excited states under study. The AO expansion for H^++-Li($2s$) collisions (AO65_64 in Table I) has been tailored to fulfill this rule for all excitation processes Li($2s$-nl) ($n=2-4$, $l=0-3$). A considerable enlargement of the basis size would have been necessary in the case of He^{2+} impact (AO87_79 and AO81_80 in Table I), but could not be realized because of computational reasons. In view of this, no convergent results can be expected for Li($2s$-$5l$) excitation cross sections, because the He II orbitals dominantly populated by SEC from Li($5l$) will have n values of 7–9, which is beyond the ones included in the present AO calculations.

These AOCC calculations shall be compared with all available experimental data and available theoretical calculations. By default, all theoretical curves are displayed as lines, even though they were all calculated for discrete energies.

III. EXPERIMENTAL RESULTS

The He^{2+} and H^+ ions were produced by the electron cyclotron resonance ion source (ECRIS) installed at the KVI in Groningen. The source was operated at voltages ranging from 4 to 24 kV. We also had the possibility to post-accelerate the ions with voltages of 30 to 100 kV. For our experiments this option implied a critical loss (factor of ten) in current. Typical currents for the He^{2+} and H^+ ions at the collision center (non-post-accelerated beams) were ranging from 0.5 μA at the lowest energies to 3 μA at the highest energies.

After collimation of the beam to 1 mm, the ions were crossed in the collision center with a lithium beam coming from a single stage oven [6,21] operated at a fixed temperature in the 480–520 °C range. A liquid-N_2–cooled trap was used to reduce the lithium background pressure.

The light emitted by the deexciting lithium was detected perpendicularly to the ion beam with a monochromator for visible light (320–610 nm). This (Leiss) monochromator can scan across the lithium target along the ion beam axis, which allows us to select the area with the (apparent) highest lithium density. It also allows us to distinguish the background gas contributions from the lithium signal.

The sensitivity of the monochromator for the different wavelengths was calibrated relatively using (unpolarized) light of a quartz-iodine lamp at 200 W [22]. The relative sensitivity was put on an absolute scale by using known electron impact excitation cross sections [23]. The LiI($4s$-$2p$) emission after He^{2+} impact was determined for energies in the range of 1.5–9 keV/amu, all relative to each other and relative to the LiI($4s$-$2p$) emission after 400 eV electron impact [note that the LiI($4s$-$2p$) emission was also chosen because it is unpolarized]. The uncertainty of our absolute calibration is 20% for wavelengths longer than 400 nm and increases to about 25% at 320 nm (see also [21]). These systematic uncertainties are not included in the error bars displayed in the figures.

For H^+, the emission cross sections were absolutely calibrated by measuring the LiI($4d$-$2p$) emission after 6 keV/amu He^{2+} impact before or after a measurement. The larger scatter in the proton impact data is caused by the (relatively long) time needed for switching from the proton beam to the reference He^{2+} beam. Relative density uncertainties (i.e., the always present oven fluctuations) were monitored by measuring a reference line [the LiI($4d$-$2p$) line] as often as possible and by measuring emission lines more than once. In the case of the weakest emission lines [LiI(ns-$2p$,$n=5,6$)], the uncertainty in the cross section is not only determined by the counting statistics, but also by the fact that the oven behavior was not monitored for a relatively long period.

To compare our measurements with theory, the theoretical excitation cross sections had to be transformed into emission cross sections. For this procedure, the following relations were used:

$$\sigma(3p\rightarrow 2s)=(0.215\pm 0.02)[\sigma(3p)+0.425\sigma(4s)+0.23\sigma(4d)], \quad (2)$$

$$\sigma(3d\rightarrow 2p)=\sigma(3d)+0.2\sigma(4p)+\sigma(4f), \quad (3)$$

$$\sigma(4s\rightarrow 2p)=0.575[\sigma(4s)+0.28\sigma(4p)], \quad (4)$$

$$\sigma(4d\rightarrow 2p)=0.77\sigma(4d), \quad (5)$$

$$\sigma(5s\rightarrow 2p)=0.48\sigma(5s), \quad (6)$$

$$\sigma(5d\rightarrow 2p)=0.71\sigma(5d), \quad (7)$$

$$\sigma(6s\rightarrow 2p)=0.43\sigma(6s), \tag{8}$$

$$\sigma(6d\rightarrow 2p)=0.65\sigma(6d). \tag{9}$$

For these relations, branching ratios from Wiese *et al.* [28] and Lindgård and Nielsen [29] are used [Wiese *et al.*, Eqs. (2)–(5), and Lindgård and Nielsen, Eqs. (6)–(9)]. There is some uncertainty concerning the lifetime of the Li($3p$) level [28–30] causing the $3p\rightarrow 2s$ branching ratio to range from 0.195 to 0.235.

The sensitivity of the monochromator for the linear polarization of the incoming light was determined with the quatziodine lamp, by adding a linear polarizer to the signal path (see also Schippers *et al.* [24]). Polarized light emissions affect our measurements in two ways: (a) the radiation will be emitted anisotropically since we do not measure at the magic angle of observation (54.7°), (b) the detector sensitivity depends on the linear polarization of the incoming light. In the case of the LiI($3d$-$2p$), these two effects work in the same direction and for all other lines the two effects work in opposite directions and effectively cancel out. Therefore, for an estimation of the maximal polarization induced uncertainty, the Li($3d$) m-level distributions of AO87_79 were used to calculate the linear polarization of the LiI($3d$-$2p$) emission after He^{2+} impact. These calculated polarizations were then used to correct the theoretical LiI($3d$-$2p$) emission cross sections. Thus this corrected curve (thin dashed line in Fig. 5) serves as an indication of the maximal uncertainty induced by neglecting the experimental linear polarization sensitivity of our setup.

Although we treated the linear polarization of the emitted light as a source of experimental uncertainties, it in principle a source of information about the collision dynamics (i.e., the m-level population of the states of interest). Schippers *et al.* [25] measured the only reported case, the linear polarization of NaI($3p$-$3s$) emission in the case of Na excitation. The polarization of emission after electron capture is, however, more widely studied, for example, by Laulhé *et al.* [26] (electron capture from Li) and Grego *et al.* [27] (electron capture from Na).

A. Proton impact

In this section, the proton impact data will be discussed with their AO simulations (and other available data) as separate cases. The LiI($5d$-$2p$) data will be shown in this section only to get an impression of the physics of target excitation. Later on, in Sec. IV, they will be evaluated more quantitatively together with the He^{2+} impact case.

All error bars are at least 15% because of the relative uncertainty associated with the calibration procedure. Some other lines, LiI($3d$-$2p$), LiI($5s$-$2p$), and LiI($6d$-$2p$), also have an additional 5–15 % statistical uncertainty. [Note: Our detector was 50 times less sensitive at the LiI($3d$-$2p$) wavelength (610 nm) than at the LiI($4d$-$2p$) (460 nm).] Also the LiI($3p$-$2s$) has an enhanced uncertainty of at least 10% because, at 323.3 nm, it is at the very edge of our detection range.

1. LiI(3d-2p) emission after proton impact

The LiI($3d$-$2p$) emission cross section measured by us, the experimental data from Brandenburg *et al.* [15], and the AO calculations are shown in Fig. 1. The AO results agree well (within our experimental uncertainties) with the measurements. The good agreement of our LiI($3d$-$2p$) emission cross sections with the corresponding experimental data from Vienna confirms the correctness of our independent calibration method. Also shown is the recommended curve from Wutte *et al.* [17] (excitation only, because cascade contributions could not be incorporated). In the high-energy limit ($E\geqslant 20$ keV/amu) all curves converge, but in the 3–10 keV/amu range, the region of interest for plasma diagnostics, discrepancies by a factor of 3 can be seen. It is quite clear that the reason for this discrepancy [the depletion of Li($2s$-$3d$) excitation channel around 4 keV/amu] should be the dominance of the electron capture channel in this energy range [19]. Not expected was the convergence of the different data sets at the low-energy limit.

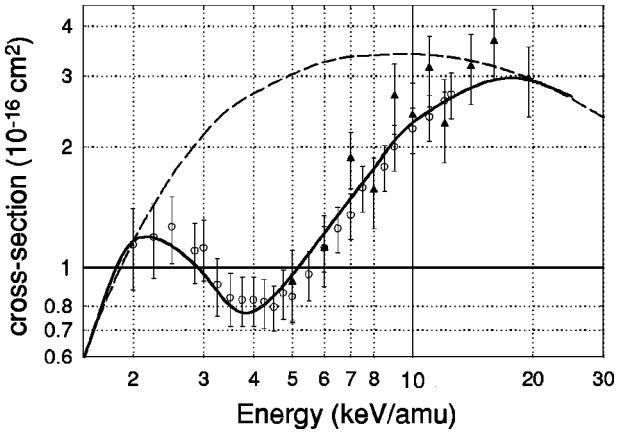

FIG. 1. LiI($3d$-$2p$) emission after H^+ impact: full triangles, this work (relative errors are shown); open symbols, Brandenburg *et al.* [15] (absolute errors are shown); full curve, ao65_64; dashed curve, Wutte *et al.* [17] (scaled electron impact emission cross sections).

2. LiI(nd-2p,n=4,5) emission after proton impact

The measured and calculated LiI($4d$-$2p$) emission cross sections are shown in Fig. 2. Fairly good agreement of experiment with theory can be observed considering that cascade contributions [mainly 0.36*Li($5f$) and 0.21*Li($5p$)

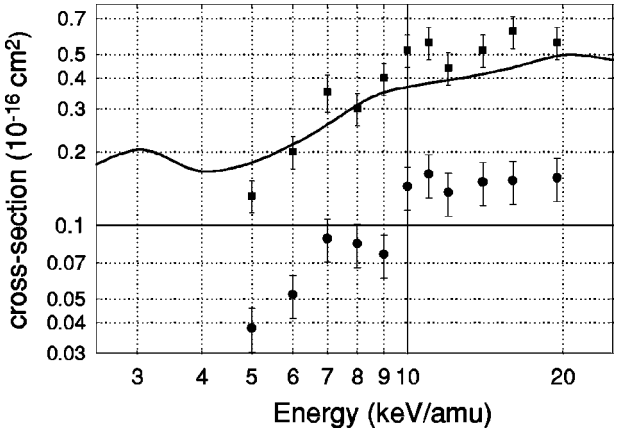

FIG. 2. LiI(nd-$2p$,$n=4$–5) emission after H^+ impact: full squares, LiI($4d$-$2p$); full curve, LiI($4d$-$2p$) ao65_64; full circles, LiI($5d$-$2p$).

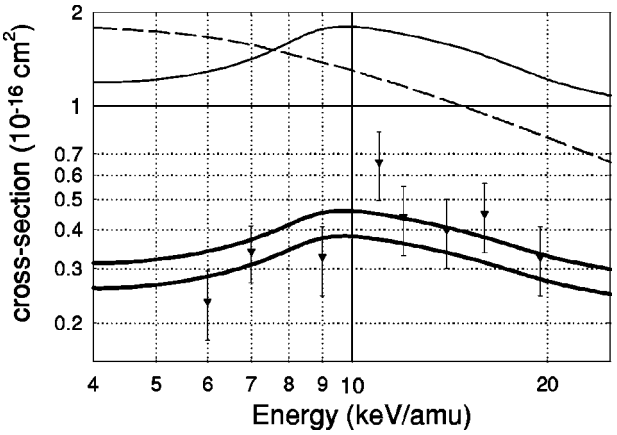

FIG. 3. LiI($3p$-$2s$) emission and Li($2s$-$3p$) excitation after H^+ impact: full symbols, LiI($3p$-$2s$); thick full curves, maximum and minimum LiI($3p$-$2s$) ao65_64; thin full curve, Li($2s$-$3p$) excitation, ao65_64; dashed curve, Li($2s$-$3p$) excitation, Wutte *et al.* [17] (scaled electron impact cross sections).

[29]] are not included in the theoretical cross sections (the estimated increase might be 10–30 %). The measurements on the LiI($5d$-$2p$) are also shown with the previously discussed LiI($4d$-$2p$) data in Fig. 2. The similarity of both emissions as a function of energy is quite striking. A quantitative analysis of these cross sections as a function of quantum number n is given in Sec. IV.

3. LiI(3p-2s) emission after proton impact

The LiI($3p$-$2s$) emission data seem to agree well with the AO simulations (Fig. 3). As already mentioned, the $3p \rightarrow 2s$ branching ratio has a large (20%) uncertainty. Two extreme cases (0.195 and 0.239) are displayed in Fig. 4, to indicate the maximum margin in the theoretical curve. Also displayed are the Li($2s \rightarrow 3p$) excitation cross sections by Wutte *et al.* and AO65_64. The agreement is quite good but shows a somewhat different trend.

4. LiI(ns-2p,n=4,5) emission after proton impact

The LiI($4s$-$2p$) and LiI($5s$-$2p$) emission cross sections are shown in Fig. 4. For impact energies $E > 10$ keV the

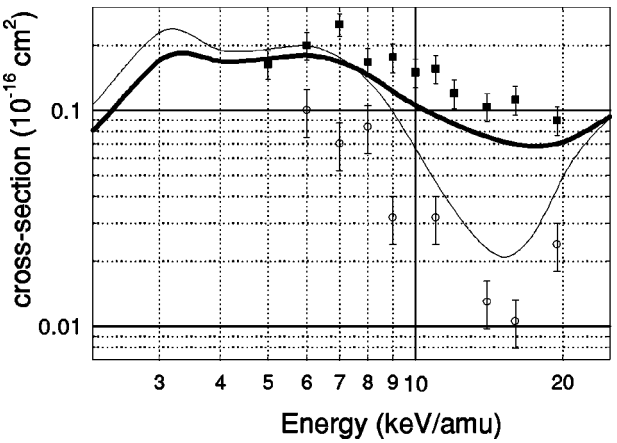

FIG. 4. LiI(ns-$2p$,$n=4,5$) emission after H^+ impact: full squares, LiI($4s$-$2p$); open circles, Li($5s$-$2p$); thick curve, LiI($4s$-$2p$), ao65_64; thin curve, Li($2s$-$4s$) excitation, ao65_64.

$4s$-$2p$ emission is dominated by the cascade contribution $4p$-$4s$. A missing cascade contribution $5d$-$4p$ in the theoretical result might be the reason for the underestimation of the experimental data. Agreement between theory and experiment, although being the worst case for the proton impact excitation, is still rather good.

The decrease of the LiI($5s$-$2p$) with increasing collision energy is at least remarkable especially when compared to all the other measured LiI emission lines. However, when compared to the AO simulations of LiI($2s$-$4s$) excitation and assuming a similarity of properties with increasing principal quantum number n, it is not so surprising. The Li($2s$-$4s$) excitation shows a deep minimum around 15 keV/amu impact energy. However, this cannot be observed in LiI($4s$-$2p$) emission measurements because of the $4p$ cascade contribution to the Li($4s$) level. Contrary to this, the LiI($5s$-$2p$) emission does not have any significant cascade contributions [Li($5p \rightarrow 5s$) = 0.15, Li($6p \rightarrow 5s$) ~ 0 [29]] and therefore this amazing decrease of the cross section becomes visible.

B. He^{2+} impact

There are more experimental results for the He^{2+} impact and they are more precisely calibrated than the proton impact data, and this proved to be a real challenge for the AOCC method. As we shall see, excellent results were obtained with the AO87_79 and good results with the AO81_80. The AO87_79 calculations include in addition to the projectile centered states of the AO81_80 the 6h state. This state was omitted only in order to reduce CPU time in the AO81_80. The target centered parts of both expansions do not differ in the AOs included, but in the number of pseudostates and in the details of the used STOs (see Table I). Especially the target centered PS-UA parts differ considerably between both expansions.

Interesting will be the lower-energy range for the He^{2+} impact data (2–12 keV/amu) as compared to the proton case (5–20 keV/amu). At these lower energies interesting ion-atom interactions were observed for the proton impact case (see the preceding section) and these are also expected for the He^{2+} impact case. Furthermore, there will be a few data points at high energies.

1. LiI(3d-2p) emission after He^{2+} impact

The most striking feature of the LiI($3d$-$2p$) emission cross sections (Fig. 5) is, as in the proton impact case, the peak at 2.7 keV/amu, which, as in the proton impact case, is likely to be caused by a depletion of the Li($3d$-$2p$) excitation channel by electron capture channels. Cross checking the present lithium emission after He^{2+} impact with electron capture from lithium by He^{2+} [21] clearly reveals that the experimental HeI($n=4$, $l=0,1,2$) (capture) levels have an enhanced population around 6 keV/amu, exactly where the Li($n=3,4$, $l=3$) (excitation) levels have reduced intensities.

We can now really see the improvements in the AOCC method, because the LiI($3d$-$2p$) emission after He^{2+} impact was studied with this method by Ermolaev *et al.* [9] and Schweinzer *et al.* [10] and these results are also displayed in Fig. 5. The previous calculation by Schweinzer *et al.* was good down to 4 keV/amu but then failed to predict the fea-

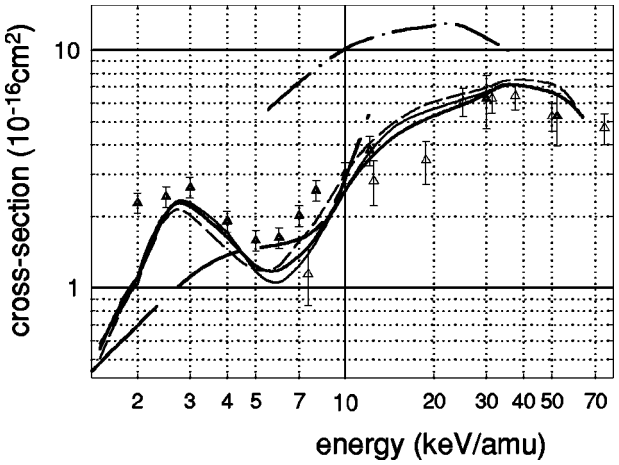

FIG. 5. LiI($3d$-$2p$) emission after He^{2+} impact: full symbols, this work (relative errors are shown); open triangles, Kadota *et al.* [6] (absolute errors are shown); thick full curve, ao87_79; dashed thin curve, ao87_79 corrected for the polarization sensitivity of the detector; thin full curve, ao81_80; thick dashed curve, Schweinzer *et al.* [10]; thick dash dot curve, Ermolaev *et al.* [9].

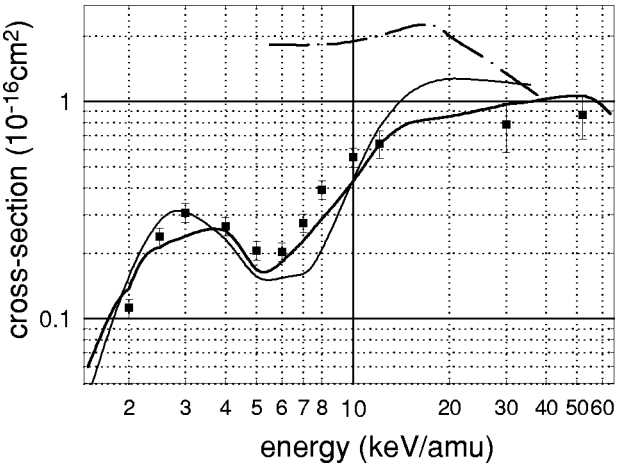

FIG. 6. LiI($4d$-$2p$) emission after He^{2+} impact: full squares, this work; thick full curve, ao87_79; thin full curve, ao81_80; dash dot curve, Ermolaev *et al.* [9].

tures so striking in Li excitation by H^+ and He^{2+} impact. The data points by Ermolaev (the AO65 calculations) only agree with our data in the high-energy limit (towards the Born regime). The pseudostate expansion applied by Ermolaev is optimized for high impact energies. Thus only a few projectile centered states (He II $n=2,3+4d$ and pseudostates) were taken into account in their calculation, leading to overestimated excitation cross sections for their lowest impact energies. On the other hand, the previous calculation by Schweinzer *et al.* is based on a pure AO expansion with many projectile centered states (He II $n=1-6$) but without pseudostates, thus completely neglecting the coupling to ionization channels. A sufficient representation of all inelastic reaction channels seems to be necessary to describe excitation processes properly.

Note that the inclusion of polarization effects (as discussed in the experimental results section) changes the emission cross sections only slightly.

2. LiI(4d-2p) emission after He^{2+} impact

The LiI($4d$-$2p$) emission cross sections are shown in Fig. 6. The agreement between the AO87_79 calculation and the experimental data is very good, except maybe at 3 keV/amu, where the AO81_80 agrees somewhat better with experiment. Differences between AO87_79 and AO81_80 give an estimate of the convergence of AOCC results. The agreement between theory and experiment is slightly better here than for the proton impact case, Fig. 2, although also here small cascade contributions to the theoretical emission curve were not included. Finally, the theoretical data by Ermolaev *et al.* (AO65 calculations) converge with our data in the high-energy limit, but again are far too high at low energies.

3. LiI(5d-2p) and LiI(6d-2p) emission after He^{2+} impact

The LiI(nd-$2p$,$n=5,6$) emission data are shown in Fig. 7. The disagreement between the experimental LiI($5d$-$2p$) data and the AO87_79, AO81_80 is very considerable (factor of 2–3), which is most probably due to the missing high-n SEC channels. As already explained in Sec. II, SEC draws flux from the excitation channels, thereby reducing the excitation cross sections. The predicted $2s$-$5d$ excitation cross sections are almost as large as the $2s$-$4d$ cross sections, which is very unlikely. Also Ermolaev *et al.* struggled with the problem of excessively large Li($2s$-$5d$) excitation cross sections due to the even lower number of SEC channels, and their best results are displayed in Fig. 7.

Also shown are the LiI($6d$-$2p$) emission cross sections (experiment only). It is clear that this emission line looks quite similar to the other LiI(nd-$2p$) emissions, although the peak structure at 3 keV/amu (minimum around 6 keV/amu) seems to have disappeared.

4. LiI(3p-2s) emission after He^{2+} impact

For the LiI($3p$-$2s$) emission cross section, the agreement between the experimental data and the AO simulations, both AO87_79 and AO81_80, is reasonably good (see Fig. 8; a branching ratio of 0.215 was used for the theoretical curve).

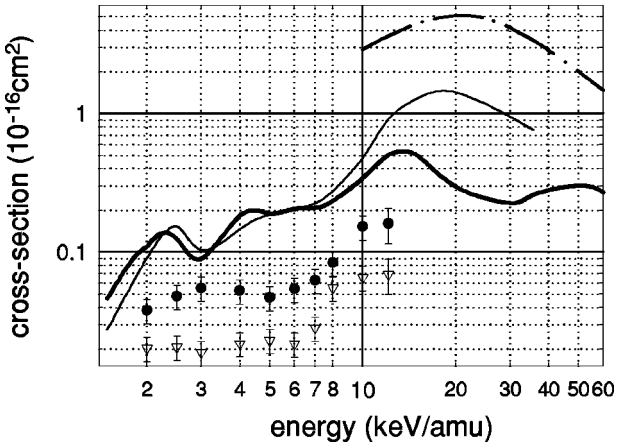

FIG. 7. LiI(nd-$2p$,$n=5,6$) emission after He^{2+} impact: full circles, LiI($5d$-$2p$); open triangles, LiI($6d$-$2p$); thick full curve, ao87_79; thin full curve, ao81_80; dash dot curve, Ermolaev *et al.* [9].

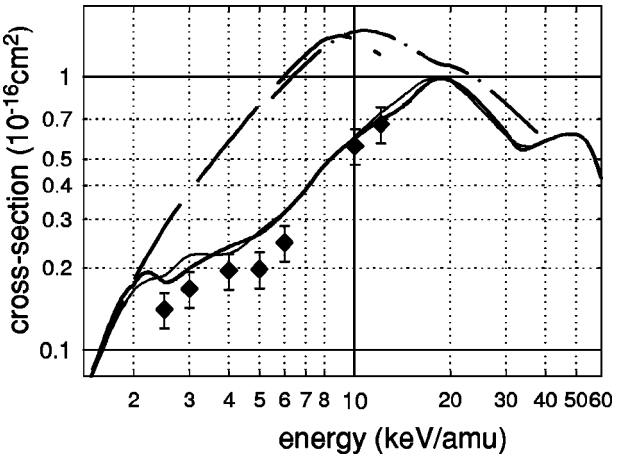

FIG. 8. LiI($3p$-$2s$) emission after He^{2+}impact: full symbols, LiI($3p$-$2s$); thick full curve, LiI($3p$-$2s$) ao87_79; thin full curve, ao81_80; dashed curve, Li($3p$-$2s$), Schweinzer *et al.* [10]; dash-dot curve, Ermolaev *et al.* [9].

5. LiI(4s-2p) emission after He^{2+} impact

We can see in Fig. 9 that the LiI($4s$-$2p$) emission after He^{2+} impact, which is our basis of absolute calibration, agrees well with the AOCC theory (except maybe for a small structure at 3 keV/amu). The experimental LiI($4s$-$2p$) emission cross sections are almost featureless between 1.5 and 10 keV/amu. This is of importance since this line is the reference for all other He^{2+} emission lines (lines which have distinct features below 10 keV/amu). Our calibration method therefore cannot have introduced phantom features into the various He^{2+} impact emission cross sections. (Note that if we would have measured the 3 keV/amu cross section as predicted by the AOCC simulations, the 3 keV/amu cross sections in Figs. 5 and 6 would have been $\sim$70% higher.) Also shown is the calculated Li($2s$-$4s$) excitation to show that a minimum above 12 keV/amu (as seen for H^+) also exists for He^{2+} impact.

6. LiI(5s-2p) and LiI(6s-2p) emission after He^{2+} impact

The theoretical and experimental results for LiI($5s$-$2p$) can be seen in Fig. 10. Clearly the agreement of the

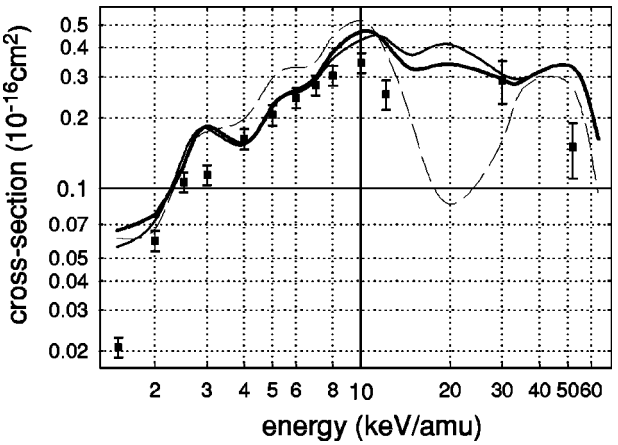

FIG. 9. LiI($4s$-$2p$) emission after He^{2+} impact: full squares, LiI($4s$-$2p$); thick full curve, ao87_79; thin full curve, ao81_80; dashed curve, Li($2s$-$4s$) excitation, ao87_79.

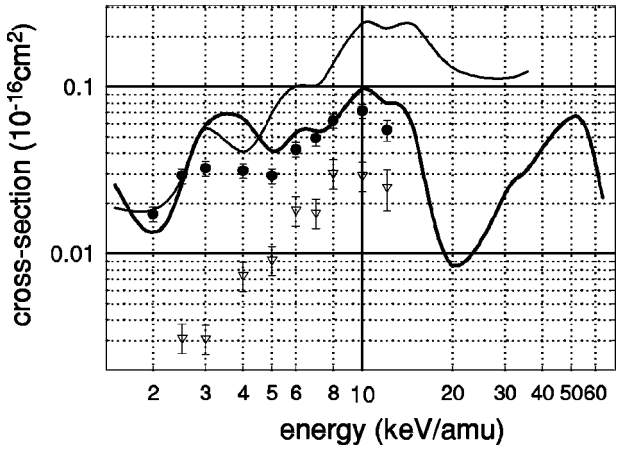

FIG. 10. LiI(ns-$2p$,n=5,6) emission after He^{2+} impact: full circles, LiI($5s$-$2p$); open triangles, LiI($6s$-$2p$); thick full curve, ao87_79; thin full curve, ao81_80.

AO87_79 with experiment is much better than in the LiI($5d$-$2p$) case (Fig. 7). The $5s$ level is slightly tighter bound than the $5d$ state. Therefore, SEC from the Li($5s$) state is better represented in the AO calculations than SEC from Li($5d$).

Results of the AO81_80 calculation, as well as the AO87_79 data, are above the experimental values. The significant difference between both calculations, especially at higher impact energies, might be due to the missing He II($6h$) state in the AO81_80 expansion. Although this state is populated very weakly in collisions with Li($2s$), it might be of considerable importance as a SEC loss channel from Li($5s$). To test the idea that the He II($6h$) capture channel interferes with the Li($5s$) excitation channel, an AO87_80 [an AO81_80 plus the He II($6h$) state] calculation was performed. This calculation, however, did not result in a better description of the Li($5s$) excitation channel, implying that the AO87_79 is more successful in the prediction of Li($5s$) excitation because of a better choice of pseudostates describing the ionization channels. The AO87_79 is definitely more successful when it comes down to describing the dramatic decoupling (decoupling meaning the excitation mechanism is becoming less effective) of the Li($5s$) excitation channel above 12 keV/amu [remember, this peculiar behavior of the Li($5s$) excitation was also seen for proton impact].

Also displayed in Fig. 10 are the LiI($6s$-$2p$) emission cross sections (experiment only). It is clear that this excitation channel behaves differently from the Li($5s$) excitation. This indicates that a universal scaling law for describing LiI(ns-$2p$, $n=4-6$) emissions (He^{2+} impact) is unlikely to exist.

IV. LiI(nd-$2P$,$n=3-9$) EMISSION: SCALING TO QUANTUM NUMBER n

As far as we know, the field of ''high-n excitation by ion impact'' is unknown territory. To get some idea of the mechanisms at work, some extra measurements have been performed and a crude scaling method is introduced for the nd states. It is custom in the field of fusion plasma diagnostics to find scaling relations because it is a formidable (if not

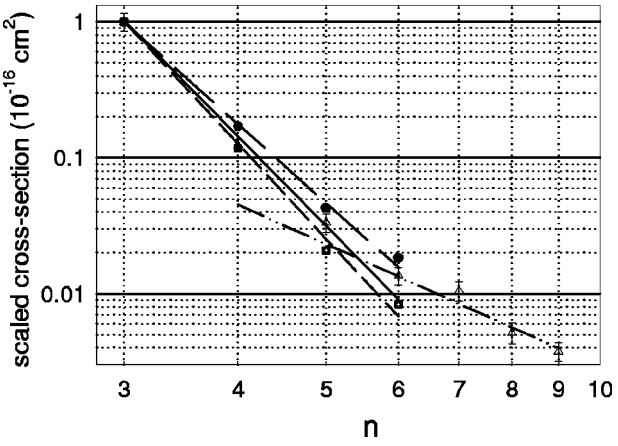

FIG. 11. Normalized (scaled) LiI(nd-$2p$,$n=3,9$) emission after He^{2+} impact: full circles, 12 keV/amu; open triangles, 6 keV/amu; full squares with dot, 3 keV/amu (relative error are shown); full curve, $n^{-6.8}$ line; long dashed curve, n^{-6} line; short dashed curve, $n^{-7.2}$ line; dash dot dot curve, n^{-3} line.

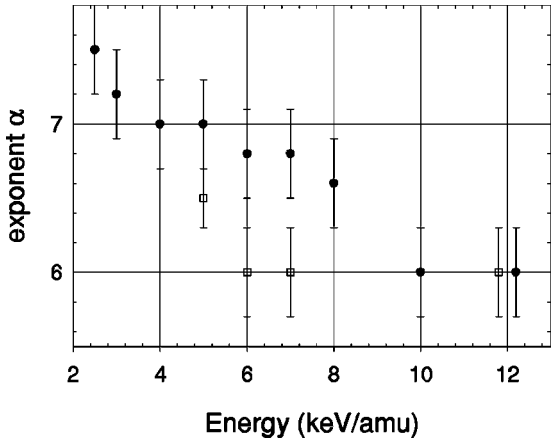

FIG. 12. Behavior of the exponent α (see text and the lines in Fig. 12) versus energy: full circles, He^{2+}; open squares, H^+.

impossible) task to measure or calculate all the relevant cross sections for inelastic ion-atom collisions. As already mentioned before, lithium ns-state excitation by ion impact is not suitable for scaling with increasing n (the curves in Figs. 4, 9, and 10 simply do not look very similar).

In Fig. 11 the result can be seen of plotting the (He^{2+} impact) LiI(nd-$2p$,$n=3$–9) emission cross sections versus quantum number n (for just three energies). For clarity reasons, the error bars are only drawn for the 6 keV/amu case.

When the emission cross sections are plotted on a double logarithmic scale, straight lines can be drawn, each line indicating a certain $n^{-\alpha}$ behavior for the cross sections (with n the principal quantum number). All these straight lines are normalized to the first data point [the LiI($3d$-$2p$) emission cross sections]. This fit indicates that the systematic error in the measured LiI($5d$-$2p$) emission cross sections is probably not very large [this as a supplement to the discussion about the disagreement of the experimental and the theoretical LiI($5d$-$2p$) data in Sec. III C].

For the LiI(nd-$2p$,$n=6$–9) emission cross sections at (6 keV/amu) (Fig. 11), an n^{-3} dependence can be fitted to the data [starting at LiI($6d$-$2p$) or LiI($7d$-$2p$)]. This n^{-3} behavior is also observed in (lithium) target emission after electron impact and is regarded as a ''trademark'' for hydrogenic behavior, i.e., the n^{-2} dependence of the hydrogenic binding energies results in a density of states $\partial E/\partial n = \text{const} \times n^{-3}$.

The scaling procedure was also performed for the proton impact experimental data with comparable results. Again, as for the He^{2+} impact case, it is striking how well the data can be fitted with these $n^{-\alpha}$ lines, even though the data span two orders of magnitude.

Putting the results (the exponents α) of the $n^{-\alpha}$ fits, both for He^{2+} and H^+ impact, in a plot yields Fig. 12. The physical origin of the decrease of the exponent α with increasing collision energy is more or less clear. It is expected that the higher Li(nd) states are relatively stronger populated when the projectile energy increases. Interesting is, however, that the H^+ and He^{2+} projectiles have (more or less) the same exponent ($\alpha \sim 6$) at their highest energies, but the protons reach that exponent sooner. Putting it simply, at high enough velocities, both projectiles can ''pump'' the relative nd populations equally well; the protons, however, can do this ''pumping'' already better at lower energies.

V. CONCLUSION

In this work we have seen that the AOCC method can model the excitation of lithium atoms by H^+ or He^{2+} with great accuracy not only for the dominant channels [Li($2p$) described in [14] and Li($3p$,$3d$)] but also for excitation channels that are two orders of magnitude below these channels. By comparing experimental data for even smaller cross sections with AOCC calculations, although already of large scale, limitations [Li($5d$) excitation] have been reached and disagreement was observed. However, the reason for the failure is rather clear and can be overcome by a further enlargement of the basis. However, such extensions are not only a matter of more powerful computers, but will also need improved numerical methods, because accuracy limits of the present ones are also touched upon.

The main improvement between the old AOCC simulations (Ermolaev *et al.* and Schweinzer *et al.*) and the new ones is that the new ones correctly predict the features in the Li($2s$-nd,$n=3$–4) excitation. As already mentioned in Sec. III A 1 [Li($3d$-$2p$) emission after H^+ impact], it is likely that these features are not ''peaks around 3 keV/amu'' but ''minima around 6 keV/amu.'' Similar structures, resulting from the interplay between capture and excitation, have also been predicted by Schultz *et al.* [12] and Fritsch *et al.* [11] for hydrogen excitation and experimentally seen by Aumayr *et al.* [8] (lithium and sodium excitation) and Horvath *et al.* [13] (sodium excitation). The Li($2s$–ns,$n=4,5$) excitation channels also display minima with H^+ and He^{2+} impact, not around 5 keV/amu but around 15 keV/amu for the former and 20 keV/amu for the latter. We could not find a satisfying explanation for these depletions of the Li($4s$) and Li($5s$) excitation channels above 12 keV/amu.

We would like to mention that the structures between 2 and 8 keV/amu were discussed by Aumayr [8] using the Landau-Zener picture, and a pure classical interpretation of this structure was given by Schultz [12]. Both discussions construct a picture of the active electron oscillating (or swap-

ping) between excitation and capture channels, resulting in the typical structures observed. Although we clearly saw depletion of excitation channels due to enhanced capture, we did not find any evidence for the reverse process (i.e., enhanced excitation and depleted capture channels).

We also saw that above 20–30 keV/amu the lithium excitation is governed by (Born-type) single step excitation and that below 2 keV/amu the excitation completely decouples (i.e., vanishes). Remarkably enough, not only the high-energy end but also the low-energy end can be predicted correctly by scaling electron impact excitation cross sections.

We observed that the LiI(nd-$2p$,$n=3$–9) emission, which cannot be calculated when $n>5$, can be described (i.e., scaled with quantum number n) quite successfully with power-law ($n^{-\alpha}$, $-7.5<\alpha<-6$) dependences. The LiI(ns-$2p$,$n=4$–6) could not be described with these power-law dependences.

ACKNOWLEDGMENTS

This work has been performed within the framework of the FOM-EURATOM association agreement. This work is also part of the research program of the Stichting voor Fundamenteel Onderzoek der Materie (FOM) with financial support from the Nederlandse Organisatie voor Wetenschappelijk Onderzoek (NWO). D.M. was supported by the EU TMR program, Grant No. ERBFMBICT972241.

[1] H. Ryufuku, K. Sasaki, and T. Watanabe, Phys. Rev. A **21**, 745 (1980).
[2] L. D. Landau, J. Phys. (USSR) **2**, 46 (1932); C. Zener, Proc. R. Soc. London, Ser. A. **137**, 696 (1932).
[3] A. Abrines and I. C. Percival, Proc. Phys. Soc. London **88**, 861 (1966).
[4] R. E. Olson, J. Pascale, and R. Hoekstra, J. Phys. B **25**, 4241 (1992).
[5] W. Fritsch, and C. D. Lin, Phys. Rep. **202**, 1 (1991).
[6] K. Kadota, D. Dijkkamp, R. L. van der Woude, Pan Guang Yan, and F. J. de Heer, J. Phys. B **15**, 3297 (1982).
[7] F. Aumayr, M. Fehringer, and H. P. Winter, J. Phys. B **17**, 4185 (1984).
[8] F. Aumayr, G. Lakits, and H. P. Winter, Z. Phys. D **6**, 145 (1987).
[9] A. M. Ermolaev, R. N. Hewitt, R. Shingal, and M. R. McDowell, J. Phys. B **20**, 4507 (1987).
[10] J. Schweinzer, D. Wutte, and H. P. Winter, J. Phys. B **27**, 137 (1994).
[11] W. Fritsch, R. Shingal, and C. D. Lin, Phys. Rev. A **44**, 5686 (1991).
[12] D. R. Schultz, C. O. Reinhold, and P. S. Krstic, Phys. Rev. Lett. **78**, 2720 (1997).
[13] G. Horvath, J. Schweinzer, H. P. Winter, and F. Aumayr, Phys. Rev. A **54**, 3022 (1996).
[14] R. Brandenburg, J. Schweinzer, F. Aumayr, and H. P. Winter, J. Phys. B **31**, 2585 (1998).
[15] R. Brandenburg, J. Schweinzer, S. Fiedler, F. Aumayr, and H. P. Winter, Plasma Phys. Controlled Fusion **41**, 471 (1999).
[16] J. Schweinzer, E. Wolfrum, F. Aumayr, M. Pöckl, H. P. Winter, R. P. Schorn, E. Hintz, and A. Unterreiter, Plasma Phys. Controlled Fusion **34**, 1173 (1992).
[17] D. Wutte, R. K. Janev, F. Aumayr, M. Schneider, J. Schweinzer, J. J. Smith, and H. P. Winter, At. Data Nucl. Data Tables **65**, 155 (1997).
[18] J. Schweinzer, R. Brandenburg, I. Bray, R. Hoekstra, F. Aumayr, R. K. Janev, and H. P. Winter, At. Data Nucl. Data Tables **72**, 239 (1999).
[19] M. Gieler, F. Aumayr, P. Ziegelwanger, and H. P. Winter, Phys. Rev. A **43**, 127 (1991).
[20] G. Peach, H. E. Saraph, and M. J. Seaton, J. Phys. B **21**, 3669 (1998).
[21] R. Hoekstra, E. Wolfrum, J. P. M. Beijers, H. P. Winter, and R. Morgenstern, J. Phys. B **25**, 2587 (1992).
[22] R. Stair, W. E. Schneider, and J. K. Jackson, Appl. Opt. **11**, 1151 (1963).
[23] D. Leep and A. Gallagher, Phys. Rev. A **10**, 1082 (1974).
[24] S. Schippers, P. Boduch, J. van Buchem, F. W. Bliek, R. Hoekstra, R. Morgenstern, and R. E. Olson, J. Phys. B **28**, 3271 (1995).
[25] S. Schippers, R. Hoekstra, R. Morgenstern, and R. E. Olson, J. Phys. B **29**, 2819 (1996).
[26] C. Laulhé, E. Jaquet, P. Boduch, M. Chantepie, G. Cremer, N. Gherardi, X. Husson, D. Lecler, and J. Pascale, J. Phys. B **30**, 1517 (1997).
[27] S. Grego, J. Salgado, J. W. Thomsen, M. Machholm, S. E. Nielsen, and N. Andersen, J. Phys. B **31**, 3419 (1998).
[28] W. L. Wiese, M. W. Smith, and B. M. Glennon, *Atomic Transition Probabilities*, NSRDS-NBS4 (U.S. GPO, Washington, D.C., 1966), Vol. 1.
[29] A. Lindgård and S. E. Nielsen, At. Data Nucl. Data Tables **19**, 533 (1977).
[30] D. A. Verner, E. M. Verner, and G. F. Ferland, At. Data Nucl. Data Tables **64**, 1 (1996).